Robust natural nanocomposites realizing unprecedented ultrafast precise molecular separations

Yanqiu Zhang[a], Xiquan Cheng[b], Xu Jiang[a], Jeffrey J Urban[d], Cher Hon Lau*[c], Shaoqin Liu[e], Lu Shao*[a,d]

ChemSusChem Communications Dedication

Abstract: Synthetic polymer membranes can potentially reduce the large energy and carbon footprints that are typically associated with traditional chemical separation technologies. Unfortunately, current production protocols negate the green benefits of membrane separation. To address this bottleneck, here we report the use of natural materials such as polydopamine and a monosaccharide – glucose and Zr-based metal organic frameworks (MOFs) to fabricate thin-film nanocomposite membranes via interfacial-confined reaction. Most importantly, we demonstrate such natural-driven nanocomposite membranes enables ultra-stability even in polar aprotic solvents, and ultra-fast, low-pressure, precise separations in both nanofiltration modes, which easily surpassing state-of-the-art membranes.

Introduction

Advanced separation techniques are crucial for environmental remediation where industrial wastewater is treated before discharge[1] and in the production of potable water. The principle underpinning separation processes in these applications is based on the removal of molecular compounds such as heavy metal ions, dyes, and salts from water and organic liquids using a driving force. This can be achieved with a phase change where the liquid is boiled off leaving the molecular solids behind i.e. distillation.[2] Alternatively, pressure can be employed as a driving force to achieve the same effect using membranes, but with significantly lower energy consumption (as much as 90 % lower).[3] To realize this potential, membranes must have excellent transport characteristics, and maintain separation regardless of operating conditions and environment. This is typically achieved with synthetic polymers that are produced using complex protocols[4] and hydrocarbon resources that are fast-depleting.[5] This can be overcome with polymers of natural compounds.

The first commercial polymer membrane was fabricated in the 1960s using cellulose acetate, a fucntionalized natural polymer, for the production of potable water *via* reverse osmosis desalination.[6] With excellent chemical resistance, cellulose acetate membranes are preferred for commercial settings.[7] The strategy to optimize the green benefits of advanced separation technique is to develop membranes in a green manner by replacing synthetic polymers with natural, renewable materials.[8] This strategy draws inspiration from the ongoing replacement of polystyrene or polyethylene packaging with biodegradable poly(lactic acid),[9] and using cellulose membranes to purify water/oil mixtures.[10] However, this approach is seldom demonstrated for organic solvent nanofiltration (OSN) [11] as most natural materials are unstable in polar organic solvents and whilst demonstrating low solvent permeances. For example, polyesters derived from gallic acid and polyamides produced from tannic acid[12] demonstrated good water permeances and excellent selectivity towards inorganic salts but were not resistant to organic solvents. Likewise, membranes fabricated from polydopamine (pDA), an mussels inspired polyphenol polymer, exhibit good resistance to salts whilst remaining stable in organic liquids, enabling application in organic solvent nanofiltration.[11a, 13] However, these membranes demonstrate low solvent flux as crosslinking was employed to imbue chemical stability to pDA. Clearly, there remains a trade-off relationship between chemical stability and separation performances of membrane derived from natural compounds.

Different from these approaches, here, we report that the combination of natural materials such as polydopamine (pDA), and glucose with Zr-based metal organic frameworks (MOFs) via interfacial-confined reaction can produce high-performance, multi-functional nanofiltration membranes for organic solvent nanofiltration where molecular dyes(Fig. S1 and Table S1) are separated from organic liquids during solvent recovery and in desalination to remove inorganic salts from water (Fig. 1a,b). We will demonstrate that each component of this nanofiltration membrane is crucial for yielding excellent separation performances in different media without sacrificing both selectivity and chemical stability at various operating conditions. The separation performances of our novel nanocomposite derived from natural compounds outperformed state-of-the-art MOF-

[a] MIIT Key Laboratory of Critical Materials Technology for New Energy Conversion and Storage, State Key Laboratory of Urban Water Resource and Environment (SKLUWRE), School of Chemistry and Chemical Engineering, Harbin Institute of Technology Harbin 150001, P.R. China
[b] School of Marine Science and Technology Harbin Institute of Technology Weihai 264209, P.R. China
[c] School of Engineering, The University of Edinburgh, The King's Buildings, Mayfield Road, EH9 3JL
[d] The Molecular Foundry, Lawrence Berkeley National Laboratory, Berkeley, California 94720, United States
[e] School of Life Science and Technology State Key Laboratory of Urban Water Resource and Environment Harbin Institute of Technology, Micro- and Nanotechnology Research Center Harbin Institute of Technology Harbin 150080, China

Supporting information for this article is given via a link at the end of the document.

based nanocomposite membranes (Fig. 1c and Table S2).[14] This was mainly ascribed to the synergistic effects of each component that overcome the traditional drawbacks of polymers from natural compounds – poor chemical stability, low solvent permeance and reduced selectivity. Importantly, our strategy can be extended to other natural compounds with compatible functionality to produce next-generation membranes with a plethora of combinations.

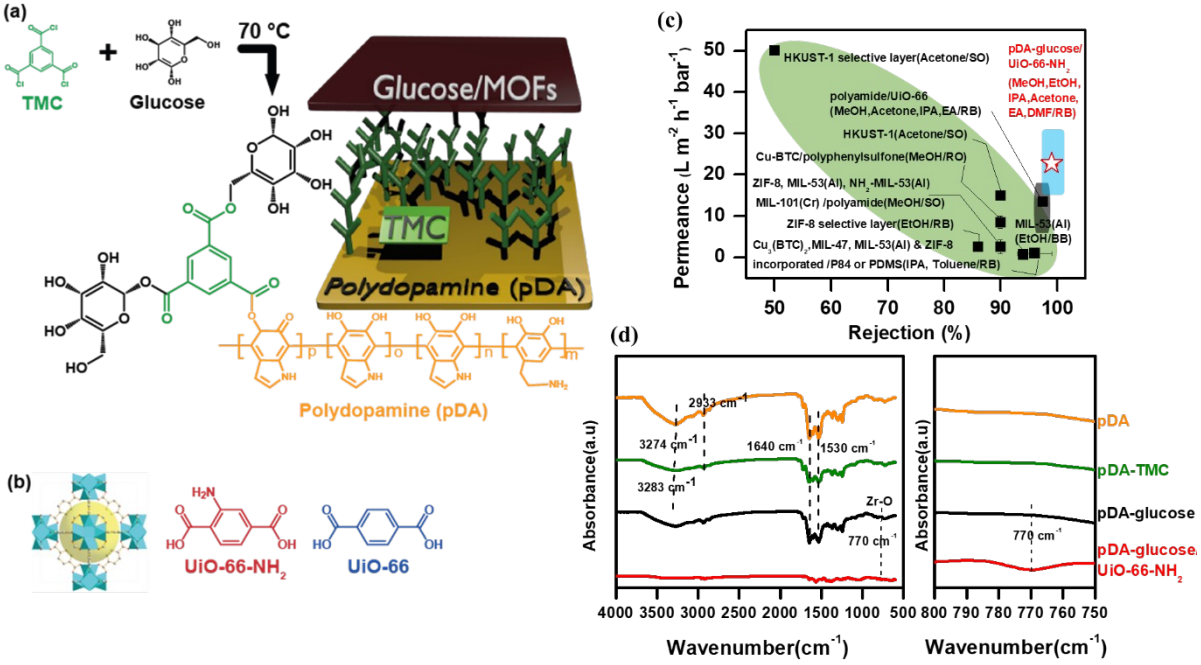

Fig. 1. (a) Cartoon showing the different components in the selective layer (pDA, glucose and MOFs) and porous substrate or support (polyimide) of the thin-film composite membranes studied in this work. In reality, the selective layer is about 214 nm thin.(b) Chemical structures of UiO-family MOFs deployed in this work – UiO-66, UiO-66-NH_2. (c) A comparison of separation performances of pDA-glucose/MOF membranes developed in this work and state-of-the-art MOF-based nanocomposite membranes for organic solvent nanofiltration.(d) FTIR analyses of pDA, pDA-TMC, pDA-glucose and pDA-glucose/MOFs thin film nanocomposite membranes developed here.

Results and Discussion

As a proof-of-concept, we employed pDA-glucose/MOF nanocomposites as 200 – 300 nm thin selective layers of thin-film composite membranes comprising porous polyimide supports (Fig. 1a,b). Glucose was chosen here for its availability, low-cost, hydrophilicity and low molecular weight that can possibly reduce the formation of non-selective voids during interfacial polymerization. MOFs are porous crystalline materials comprising metal ions linked together by organic ligands,[15] and were deployed here for their exceptional porosity that drastically enhanced solvent transport.[14a] UiO-66 and UiO-66-NH_2 MOFs [16] were chosen here for their stability in water and organic solvents. These Zr-based MOFs can also be produced at room temperature using acceptable solvents;[17] potentially contributing towards the fabrication of a green membrane. The remarkable adhesion properties of pDA[18] was harnessed here to prevent delamination of the glucose/MOF selective layer from the porous substrate and reduce macroscopic cracks during membrane fabrication. These materials were assembled into a thin selective layer via interfacial-confined reaction. This approach was adopted to produce ultrathin nanofiltration membranes with excellent molecular transportation properties. Fourier transform infra-red spectroscopy (FTIR) was deployed to verify the presence of these MOF in 214 ± 10 nm thin pDA-glucose/UiO-66-NH_2 selective layers.

Upon pDA deposition, new peaks centred at 3274 cm^{-1} and 2933 cm^{-1} were observed from the FTIR analyses (Fig. 2d). The peak at 3274 cm^{-1} correlated to the stretching vibrations of both pDA amine and phenolic -OH groups, while the peak at 2933 cm^{-1} corresponded to the $–CH_2–$ stretch in pDA. Aromatic rings of pDA contributed to peaks at 1640 cm^{-1} and 1530 cm^{-1}.[19] To facilitate subsequent coupling of glucose and MOFs, we grafted trimesoyl chloride on to the pDA layer. This resulted in a –right-shift of the peak at 3274 cm^{-1} to 3283 cm^{-1}, whilst the intensity of this peak was reduced drastically. This peak was broadened further when glucose was coupled on to the pDA-TMC(1,3,5-Benzenetricarbonyl trichloride) surface. This was due to the introduction of more –OH groups by the reaction between glucose hydroxyl group with TMC acyl chlorides or pDA. In the presence of UiO-66-NH_2 MOFs, new peaks at 770 cm^{-1} corresponding to Zr-O bonds were also observed.[20] X-ray photoelectron spectroscopy was also deployed to verify the presence of these elements (Fig. S3 and Table S3) in pDA-glucose/UiO-66-NH_2 selective layers (Fig. 2a). MOFs used here in this work were synthesized according to the work of Farha and co-

workers (Fig. S4).[16] X-ray diffraction (XRD) analyses of these MOFs consisted peaks centred at 2 positions that are characteristic of UiO-family MOFs (Fig. S5). The Brunauer-Emmett-Teller surface areas of our UiO-66, UiO-66- NH_2 MOFs were 1410 m^2 g^{-1} and 670 m^2 g^{-1} respectively (Fig. S6).

MOF additives and pDA-glucose matrix. This was elucidated here with gas adsorption analysis of UiO-66 and UiO-66-NH_2 MOFs blended with glucose. When blended with glucose, the surface area of UiO-66 MOFs was reduced by 10 % from 1410 m^2 g^{-1} to 1257 m^2 g^{-1} (Table S4). This loss in surface area was significantly

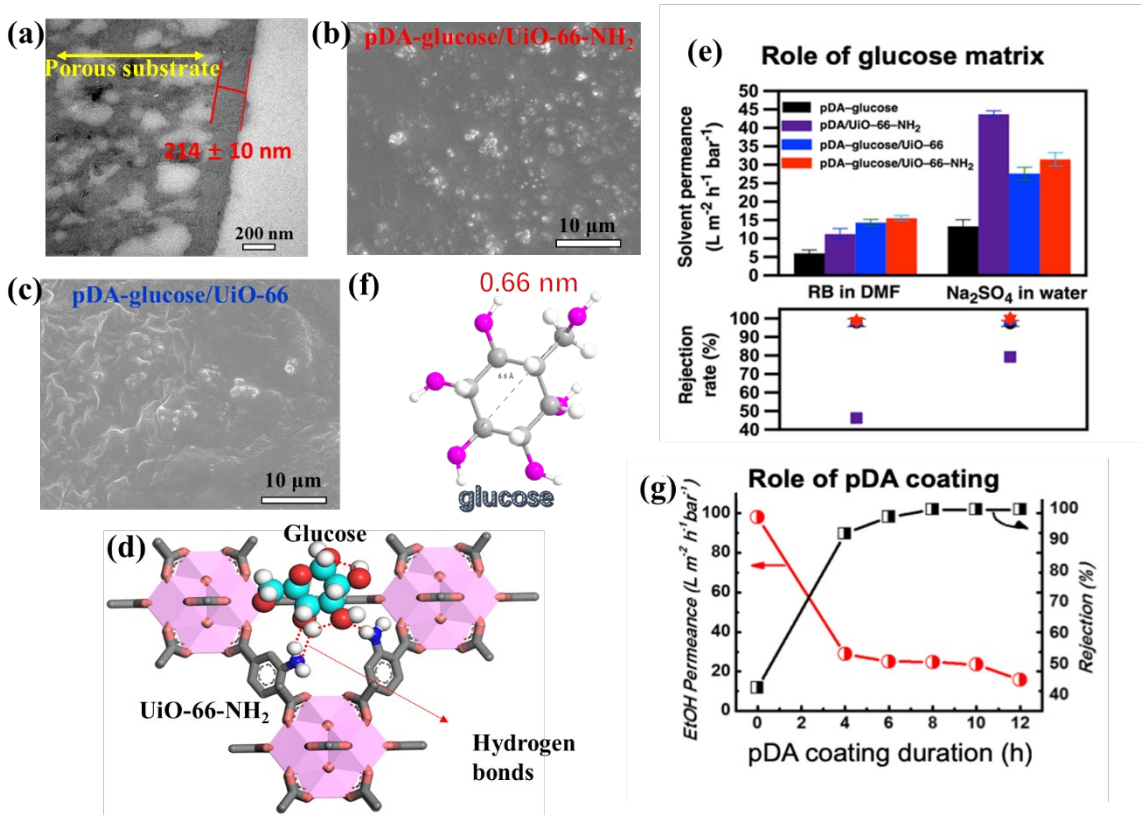

Fig. 2. (a)The average thickness of the pDA-glucose/MOF selective layers is around 214 nm.(b,c)The dispersion of UiO-family MOFs is dependent on the functional groups present. Hydrophilic NH_2 functional groups facilitate the dispersion of these Zr-based MOFs, while pristine UiO-66 MOFs tend to agglomerate. (d) MD simulations of glucose and UiO-66-NH_2 MOFs showing the preferred interactions between these components *via* hydrogen bonding. Hydrogen bonds formed between glucose and UiO-66-NH_2 segments. (Zr., pink; O in UiO-66-NH_2, magenta; C in UiO-66-NH_2, black; N, blue; C in glucose, cyan; O in glucose, red; H in glucose, white; H atoms connected to C in UiO-66-NH_2 were not shown.). The roles of (e) glucose matrix and (f) the pDA coatings are elucidated with organic solvent nanofiltration experiments using ethanol and Rose Bengal (RB) dyes at room temperature and 5 bar and nanofiltration tests with Na_2SO_4 and water. (g) Glucose molecular size is calculated using Chem 3D.

In the presence of glucose, amine functionalized UiO-66 MOFs were finely dispersed in the selective layer (Fig. 2b,c). This was due to the formation of hydrogen bonds and the amide bonds between the hydroxyl functional groups of glucose and amine groups of UiO-66-NH_2 MOFs. This was evidenced by FTIR analyses (Fig. S7) where the three –NH-C=O new peaks at 2940 cm^{-1}, 1646 cm^{-1} and 1385 cm^{-1} appeared and the relative intensities of peaks centred at 3451 cm^{-1}(-OH of glucose) were enhanced and red-shift after UiO-66-NH_2 nanoparticles interaction with glucose. Molecular dynamics simulations (Fig. 2d) validated preferential interactions between glucose and the -NH_2 functional groups where three hydrogen bonds were observed.[21] Without -NH_2 functional groups, UiO-66 agglomerated within the pDA-glucose matrix. Clearly, the amine functional groups were crucial to facilitate better interactions between the smaller than the 32 % loss in surface area of UiO-66-NH_2/glucose blends, and could be due to the interpenetration of glucose chains within the MOF pores.

To further demonstrate the role of glucose, we fabricated a pDA/MOF membrane, and compared its separation performances with similar membranes that contained glucose (Fig. 2e and Fig. S8). However, this was only feasible with UiO-66-NH_2 MOFs where only small amounts of UiO-66-NH_2 MOFs were deposited on to the pDA layer. This was due to the membrane fabrication protocol adopted here. At room temperature, there was insufficient energy to immobilize these MOFs at the membrane surface, whereas high temperatures[22] were mandatory for incorporating MOFs on to membrane surfaces or *via* simple physical blending with readily produced polymers.[23] Moreover, in our approach, UiO-66-NH_2 were unable to directly

reaction with pDA due to the trimesoyl chloride (TMC) intermediate layer. With a low concentration of UiO-66-NH_2, the RB/DMF and Na_2SO_4/water separation performances of pDA/UiO-66-NH_2 MOF membranes were drastically lower than membranes that contained glucose(Fig. 2e). The improved hydrophilicity and tunable surface charges of the separation layers by grafting a glucose molecule will lead to a high nanofiltration performance. In addition, small molecule-size glucose(6.6 Å)(Fig. 2f) can diffuse into the membrane due to the lager pore size (0.90 nm) (Fig. 4b) of pDA-TMC membrane. The covalent bonding formed between glucose with the TMC and pDA endowed the membrane with significantly stability. Clearly, each of these synergistic components – pDA, UiO-66-NH_2 MOF, and glucose are essential for creating a membrane with superior separation performances.

The hydrophilic -NH_2 groups of UiO-66-NH_2 MOFs also enhanced the zeta potential of pDA-glucose selective layers by 150%, reaching 10 mV (Fig. S9). UiO-66 MOFs only enhanced the zeta potential of pDA-glucose nanocomposites by 100%, from -20 to 0 mV. This was in-line with the impact of chemical functionalization on the zeta potentials of UiO-66 MOFs.[24] This enhancement effect was more pronounced at pH 10. The incorporation of Zr-based MOFs also reduced the hydrophilicity of the pDA-glucose selective layer (Fig. S10). The water contact angle of pristine pDA-glucose selective layers was 18.1 ± 1°, and was slightly enhanced to 25.3 ± 1.8 ° and 23.8 ± 1.5 ° in the presence of UiO-66-NH_2 and UiO-66 MOFs, respectively,which is lower than the pristine porous substrate(38.5±0.2°). Most importantly, these enhancements in both hydrophilicity and zeta potential and the intrinsic porosity of MOFs were key to the unprecedented separation performances of membranes derived from natural compounds.

pDA were also crucial for the performance of OSN membrane, which can quickly react with acyl-chloride groups at room temperature for the better distribution and the higher loading of TMC on the membrane surface for the further interfacial polymerization. [25] To confirm the crucial role of pDA, we synthesized another TFN membrane without the pDA pre-coating via the same method. UiO-66-NH_2 MOFs agglomerated at sporadic localities within the glucose matrix (Fig. S11). The separation performances of glucose/MOF nanocomposite were non-ideal (Fig. 2g) with high permeance to ethanol (98.1 L m^{-2} h^{-2} bar^{-1}) and low rejection rates (42.5 %) for Rose Bengal dyes. Although the pDA layer reduced ethanol permeance by 75 %, the rejection rate was increased to nearly 100 %. The ethanol permeance of 24.8 L m^{-2} h^{-2} bar^{-1} was comparable to state-of-the-art membranes.[14a, 14b, 14g]. This is due to the low abundance and non-uniform dispersion of TMC without pDA, which reduces glucose/ UiO-66-NH_2 interface reaction. Longer pDA deposition durations led to higher pDA content that filled up defects,[13] underpinning the significant increase in rejection rate and drastic loss in solvent permeance as the resistance to molecular transportation increased. An optimal pDA coating duration was required to optimize rejection rates by minimizing the formation of non-selective voids (Fig. 2g), whilst preventing macroscopic cracks during membrane fabrication and imbuing chemical stability to glucose in polar solvents.

Organic solvent nanofiltration (OSN) experiments were performed at 5 bar and 25 °C. It is important to point out that the high solvent permeances of our pDA-glucose/MOF membranes dispensed the need to use high operating pressures (10 to 30 bar) that are typically deployed in traditional OSN experiments.[26] Additionally, the use of low pressures can potentially further reduce the energy consumption of OSN. A range of polar solvents including methanol (MeOH), ethanol (EtOH), isopropanol (IPA), acetone, ethyl acetate (EA), and dimethylformamide (DMF) was deployed to characterize molecular transport across pDA-glucose/MOF TFN membranes (Fig. 3a). The solvent permeances of pDA-glucose membranes studied here were significantly higher than our previously reported crosslinked pDA thin film composite membrane. Polymer crosslinking usually reduces solvent transport because of denser structures.[27] UiO-66 and UiO-66-NH_2 MOFs enhanced solvent permeances without sacrificing selectivity towards dyes of different sizes, and charges. All solvent permeances including DMF were higher than 15 L m^{-2} h^{-1} bar^{-1} whilst rejecting more than 98 % Rose Bengal. The excellent dye rejection rate of MOF-loaded pDA-glucose selective layers studied here was attributed to the compatibility between glucose and UiO-66-NH_2 that inhibited the formation of non-selective pores. Meanwhile, the intrinsic porosity of MOFs also provided additional pathways for solvent transport, whilst MOF pores that are smaller than the dyes enhanced solvent/dye selectivity. Clearly, the benefits of UiO-66-NH_2 MOFs on membrane separation performances outweighed those of pristine UiO-66 MOFs.

The DMF permeance of pDA-glucose/UiO-66-NH_2 membranes reached 15.5 L m^{-2} h^{-1} bar^{-1}, significantly higher than that of thin-film polyamide [28] and TiO_2 membranes.[29] The separation performances of our membranes were characterized using polar protic (EtOH) and aprotic (DMF) systems that contained a series of dye molecules with different sizes (molecular weight ranging from 407 to 1017 Daltons) and charges (+1 to -2). Amongst all membranes studied here, pDA-glucose/ UiO-66-NH_2 membranes demonstrated the highest DMF and EtOH permeances and highest dye rejection rates (Fig. 3b,c); surpassing state-of-the-art covalent organic framework membranes[30] and nanometer-thin films of polymers with enhanced microporosity.[31] The negative zeta potential of pDA-glucose/UiO-66-NH_2 membranes was key to the preference towards rejecting negatively charged dyes (Acid Fuschin – -2, Orange G – -2, Methyl Blue – -2, and Rose Bengal – -2) over neutral

(Bromothylmol Blue) and positively charged (Crystal Violet – +1) dyes; highlighting the role of Donnan effects.[32]

The EtOH and acetone permeances of pDA-glucose/UiO-66-NH_2 membranes were further enhanced after DMF activation. EtOH permeance increased by 22 %, from 24.8 L m^{-2} h^{-1} bar^{-1} to 30.2 L m^{-2} h^{-1} bar^{-1}, while acetone permeance was increased by 15 % without compromising rejection rates (Fig. 3d). DMF activation could have removed small oligomeric/polymeric fragments trapped within the porous PI support;[33] generating an open structure and optimized membrane structure that further enhanced solvent transport (Fig. 3e,f). The average roughness (Ra) and root mean square roughness (Rq) of pDA-glucose/UiO-66-NH_2 membranes were reduced after DMF activation. During DMF immersion, the selective layer swelled, and relaxed the undulated surface topological features, leading to structural rearrangement and reduced surface roughness.[34] This molecular-level manipulation of the membrane sub-structure underpinned the increments in solvent permeances in DMF-activated pDA-glucose/UiO-66-NH_2 membranes. Without MOF nanoparticles, the dye rejection rates and solvent permeances of pDA-glucose membranes were reduced in both acetone and EtOH systems. More importantly, the excellent separation performances of pDA-glucose/MOF membranes studied here were maintained in continuous long-term operation for 50 h of EtOH before/after DMF activation and 240 h for DMF; highlighting performance longevity (Fig. 3g,h). This was different from traditional membranes comprising thin polyamide selective layers[33b] that were prone to physical aging effects. This was probably due to the anti-ageing capabilities of polydopamine.[35] Hydrogen bonding and chemical bond between UiO-66-NH_2 MOFs and the biopolymer chains might also immobilize glucose chains.

Using a pDA-glucose membrane, we achieved a NaCl rejection rate of 79.2%. Most interestingly, the incorporation of UiO-66-NH_2 MOFs into the pDA-glucose selective layer enhanced NaCl rejection rate to 92.3 %, whilst enhancing water permeance by 114.8 %, from 18.3 L m^{-2} h^{-1} bar^{-1} to 39.3 L m^{-2} h^{-1} bar^{-1} (Fig. 4a). This observed increment in water permeance could be ascribed to the intrinsic porosity of MOFs that provided additional pathways for water transport. Meanwhile, enhanced rejections were attributed to the thicker separation layer and the relatively small pore radius (0.3 nm) which was smaller than the radii of hydrated ions (0.33 – 0.5 nm) (Fig. 4b)[36]. The selectivities of pDA-glucose/UiO-66-NH_2 membranes to 1000 ppm of inorganic salts was in the order of Na_2SO_4 (99.9%) > $MgSO_4$ (98.9%) > $MgCl_2$ (97.4%) > NaCl (92.3%). The high rejection rate of the divalent anion SO_4^{2-} of pDA-glucose/UiO-66-NH_2 nanocomposite membranes could be ascribed to the electrostatic interaction between the negatively charged membranes and divalent anions, and also the larger radii of hydrated anions (0.43 nm). The synergistic effect of size sieving and Donnan exclusion underpinned high salt rejection[37] in these membranes. Crucially, the high salt rejection rates did not compromise water permeance. Compared to state-of-the-art MOF-based nanocomposite and other high performance nanofiltration membranes, the high salt rejection rates of our pDA-glucose/MOF membranes were significantly higher (Table S5).[38] Even in the presence of 3000 ppm Na_2SO_4, the water permeances of pDA-glucose/UiO-66-NH_2 membranes reached 20.9 L m^{-2} h^{-1} bar^{-1} with 99% rejection (Fig. 4c). As desired, this membrane demonstrated extraordinary stable water filtration performance (Fig. 4d) benefiting from the exceptional stability of UiO-66-NH_2 MOF additives. No discernible degradation of membrane performance was observed during the tests around 240 h with saline solutions at the transmembrane pressure of 5 bar, further highlighting the multi-functionality of our membrane.

The separation performances of pDA-glucose/UiO-66-NH_2 membranes were also immune to biofouling – a common cause underpinning performance loss due to the build-up of biomatter on membrane surfaces (Fig. S12). Anti-fouling properties of membranes studied here were evaluated using three-cycle filtration tests and aqueous solutions containing 1g/L of bovine serum albumin (BSA) or humic acid (HA) for 1200 min. The flux recovery ratio of pDA-glucose/UiO-66-NH_2 membranes for solutions containing BSA and HA after three cycles was 90.9% and 94.9% with complete rejection and lower DR_t (15.1% for HA, 22.0% for BSA), respectively.The excellent resistance towards these hydrophobic biomolecules was due to the hydrophilic nature of the negatively-charged pDA-glucose/UiO-66-NH_2 membrane.[39] Additionally, as both BSA and HA molecules are also negatively-charged, the Donnan exclusion mechanism also contributed towards anti-biofouling characteristics.[40] Other than resistance towards biofouling and long-term operation stability, we also determined the thermal (Fig. S13) and mechanical (Fig. S14) stabilities of our pDA-glucose/UiO-66-NH_2 membranes. UiO-66-NH_2 MOFs enhanced the glass transition temperature of pDA-glucose matrices by 50º. This could be ascribed to strong hydrogen bonding and covalent bond between the glucose matrix and UiO-66-NH_2 MOFs, which was typical of these nanocomposites.[22] Compared to pDA-glucose membranes, hydrogen bonding and covalent bonding between glucose and UiO-66-NH_2 MOFs also underpinned the 45% increment in tensile strength, from 2.69 ± 0.1 MPa to 3.89 ± 0.1 MPa. Imbued with excellent mechanical stability, we also studied the separation performances of these membranes as a function of increasing operating pressure. Interestingly, higher operating pressures enhanced both the permeation and rejection rates (Fig. S15). As solvent transport across a membrane is dependent on the pressure difference between the feed and permeate streams, a higher operating pressure resulted in a larger driving force that enhanced solvent permeance. Meanwhile, the concentration gradient across the membrane dominates solute transportation, in this case Na_2SO_4. As more solvent permeates across the membrane, the solute concentration in the permeate side is further reduced; contributing to the higher rejection rate.[41] This enhanced separation performance was maintained even after 5 cycles of operation(Fig. S16).

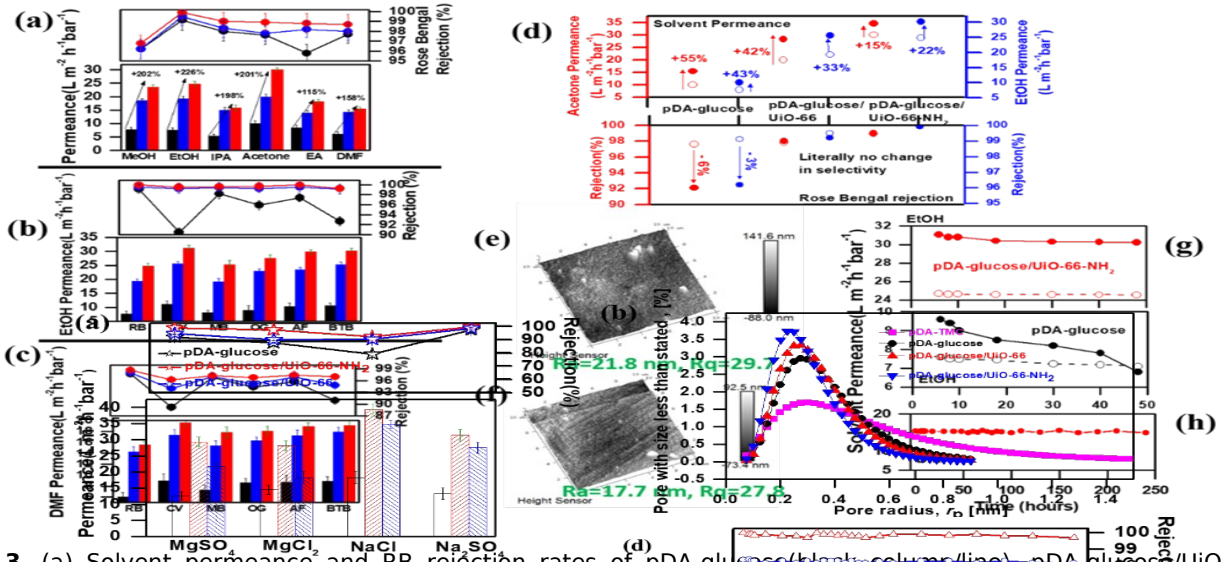

Fig. 3. (a) Solvent permeance and RB rejection rates of pDA-glucose(black column/line), pDA-glucose/UiO-66(blue column/line) and pDA-glucose/UiO-66-NH_2(red column/line) thin film nanocomposite membranes.The transport of polar solvent molecules (b) protic EtOH and (c) aprotic DMF across MOF-loaded TFN membranes.The rejection rates of various dyes in EtOH and DMF systems. (d) The EtOH and acetone permeances and RB rejection rates of the pDA-glucose, pDA-glucose/UiO-66 and pDA-glucose/UiO-66-NH_2 membranes before (blue hollow circle for ETOH, red hollow circle for acetone) and after (blue solid circle for ETOH, red solid circle for acetone) DMF activation. Change in surface roughness of pDA-glucose/UiO-66-NH_2 (e) before and (f) after DMF activation. (g) The time-dependent EtOH permeance of pDA-glucose and pDA-glucose/UiO-66-NH_2 membranes before (dotted line) and after (solid line) DMF activation. (h) The time-dependent DMF permeance of pDA-glucose/UiO-66-NH_2 (without activation) for DMF 240 h.

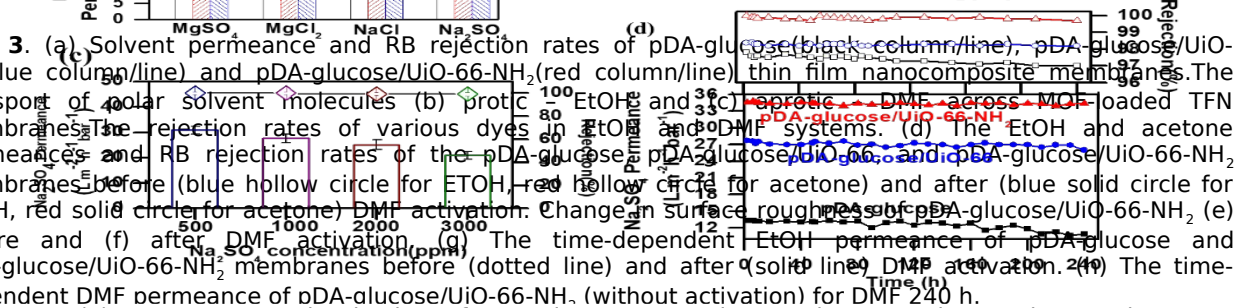

Fig. 4. (a) Permeance and rejection of pDA-glucose, pDA-glucose/UiO-66, and pDA-glucose/UiO-66-NH_2 membranes for inorganic salts aqueous solution at 5 bar. (b)The pore size distribution of the pDA-TMC, pDA-glucose, pDA-glucose/UiO-66, and pDA-glucose/UiO-66-NH_2 membranes. (c) Effects of Na_2SO_4 concentration on the performance of pDA-glucose/UiO-66-NH_2 membranes.(d) The time-dependent permeance and rejection of pDA-glucose/UiO-66-NH_2 membranes in 1000 ppm Na_2SO_4 aqueous solution.

Conclusion

In summary, we have developed a new, extendable protocol utilizing materials from sustainable natural

compounds to fabricate multi-functional, high-performance TFN membranes for fluid precise purification *via* different modes of nanofiltration. The interfacial-confined reactions of natural compounds in the presence of compatible MOF additives on the surface of synthetic porous substrates formed ultrathin selective layers. These thin film composite membranes derived from natural compounds were highly permeable whilst demonstrating excellent chemical stability. We demonstrated the multi-functionality of this membrane through realistic experimental measurements of solvent permeance and molecular/salt rejection during organic solvent nanofiltration and low-pressure desalination. The solvent permeances of these thin-film nanocomposite membranes greatly outperformed state-of-the-art membranes. This was mainly ascribed to the synergistic effects of each component that overcome the traditional drawbacks of polymers from natural compounds – poor chemical stability, low solvent permeance and reduced selectivity. Importantly, our strategy can be extended to other natural compounds with compatible functionality to produce next-generation membranes with a plethora of combinations.

Experimental Section

Porous PI substrates were prepared *via* a phase-inversion process as [42]shown in Figure S2. 0.2 g of dopamine hydrochloride was first dissolved in 100 mL of Tris buffer solution (pH=8.5, 50 mM). The porous PI substrate was immediately immersed into the dopamine solution for 8 h at room temperature. This facilitated in-situ polymerization of dopamine into polydopamine (pDA) on the surface of the PI substrate. The resulting thin-film composite pDA membrane was washed thoroughly with DI water for 0.5 h to remove any unreacted reagents, and dried in air. Subsequently, TMC was grafted on to the surface of pDA membranes using a 0.2% TMC n-hexane solution. This pDA-TMC membrane was rinsed twice with n-hexane to remove excessive TMC and n-hexane solvent. We then poured a 2% (w/v) glucose aqueous solution containing 0.2%(w/v) UiO-66-NH_2 or UiO-66 and 0.27% (w/v) DMAP on to the surface of this pDA-TMC membrane. The glucose/MOF mixture was allowed to rest on the pDA-TMC surface for 5 min. This facilitated the interpenetration of glucose/MOF solutions within the pDA layer. After 5 min, the glucose/MOF nanocomposite on the topmost surface of the pDA-TMC membrane was cured at 70 °C for 15 min – allowing nucleophilic reactions between TMC acyl chlorides and glucose hydroxyl groups. Unreacted glucose was washed from the pDA-glucose/MOF selective layer with DI water prior characterization. The glucose/MOF mixtures were stirred for more than 24 h to ensure uniform solutions with finely dispersed Zr-MOFs. A similar approach was adopted for a control sample without MOFs.

Acknowledgements

This work was supported by the National Natural Science Foundation of China (21878062). CHL acknowledges the support from the University of Edinburgh Chancellor's Fellowship. This work was partially perfomed at the Molecular Foundry, Lawrence Berkeley National Laboratory, and was supported by the Department of Energy, Office of Science, Office of Basic Energy Sciences, Scientific User Facilities Division of the U.S. Department of Energy under Contract No. DE-AC02-05CH11231.

Keywords: Dopamine • Glucose • Organic Solvent Nanofiltration • Metal Organic Frameworks • Desalination

[1] P. C. Vandevivere, R. Bianchi, W. Verstraete, *J. Chem. Technol. Biot,* **1999**, *72*, 289-302.
[2] H.-J. Huang, S. Ramaswamy, U. W. Tschirner, B. V. Ramarao, *Sep. Purif. Technol*, **2008**, *62*, 1-21.
[3] D. S. Sholl, R. P. Lively, *Nature* **2016**, *532*, 435+.
[4] M. Carta, R. Malpass-Evans, M. Croad, Y. Rogan, J. C. Jansen, P. Bernardo, F. Bazzarelli, N. B. McKeown, *Science* **2013**, *339*, 303-307.
[5] M. Höök, X. Tang, *Energ. Policy* **2013**, *52*, 797-809.
[6] S. Loeb, *Science* **1965**, *147*, 1241-1242.
[7] a) R. W. Baker, K. Lokhandwala, *Ind. Eng. Chem. Res*, **2008**, *47*, 2109-2121; b) G.D. Kang, Y.M. Cao, *Water. Res* **2012**, *46*, 584-600.
[8] R. A. Gross, B. Kalra, *Science* **2002**, *297*, 803-807.
[9] P. R. Gruber, **2001**, 166-184.
[10] K. Rohrbach, Y. Li, H. Zhu, Z. Liu, J. Dai, J. Andreasen, L. Hu, *Chem. Commun.* **2014**, *50*, 13296-13299.
[11] a) Y. Xu, F. You, H. Sun, L. Shao, *ACS. Sustain. Chem. Eng*, **2017**, *5*, 5520-5528; b) F. M. Sukma, P. Z. Çulfaz-Emecen, *J. Membr. Sci*, **2018**, *545*, 329-336.
[12] a) Y. Zhang, Y. Su, J. Peng, X. Zhao, J. Liu, J. Zhao, Z. Jiang, *J. Membr. Sci.* **2013**, *429*, 235-242; b) Q. C. Xi, X. W. Zhen, Y. Zhang, Y. Zhang, J. Ma, S. Lu, *J. Membr. Sci.* **2018**, *554*.
[13] H.C. Yang, R. Z. Waldman, M.B. Wu, J. Hou, L. Chen, S. B. Darling, Z.-K. Xu, *Adv. Funct. Mater.* **2018**, *28*, 1705327.
[14] a) S. Basu, M. Maes, A. Cano-Odena, L. Alaerts, D. E. De Vos, I. F. J. Vankelecom, *J. Membr. Sci.* **2009**, *344*, 190-198; b) S. Sorribas, P. Gorgojo, C. Téllez, J. Coronas, A. G. Livingston, *J. Am. Chem. Soc.* **2013**, *135*, 15201-15208; c) Y. Li, L. H. Wee, A. Volodin, J. A. Martens, I. F. Vankelecom, *Chem. Commun.* **2015**, *51*, 918-920; d) J. Campbell, R. Davies, D. C. Braddock, A. Livingston, *J. Mater. Chem. A* **2015**, *3*, 9668-9674; e) N. A. A. Sani, W. J. Lau, A. F. Ismail, *Rsc Adv* **2015**, *5*; f) J. Campbell, G. Székely, R. P. Davies, D. C. Braddock, A. G. Livingston, *J. Mater. Chem. A* **2014**, *2*, 9260-9271; g) L. Zhu, H. Yu, H. Zhang, J. Shen, L. Xue, C. Gao, B. V. D. Bruggen, *Rsc Adv* **2015**, *5*, 73068-73076; h) X. Cheng, X. Jiang, Y. Zhang, C. H. Lau, Z. Xie, D. Ng, S. Smith, M. R. Hill, L. Shao, *Acs Appl Mater Interfaces* **2017**.
[15] H.C. Zhou, J. R. Long, O. M. Yaghi, *Chem. Rev.* **2012**, *112*, 673-674.
[16] M. J. Katz, Z. J. Brown, Y. J. Colon, P. W. Siu, K. A. Scheidt, R. Q. Snurr, J. T. Hupp, O. K. Farha, *Chem.Comm.* **2013**, *49*, 9449-9451.
[17] M. R. DeStefano, T. Islamoglu, S. J. Garibay, J. T. Hupp, O. K. Farha, *Chem. Mater.* **2017**, *29*, 1357-1361.
[18] H. Lee, N. F. Scherer, P. B. Messersmith, *Proc. Natl. Acad. Sci. US* **2006**, *103*, 12999-13003.
[19] J. Zhao, C. Fang, Y. Zhu, G. He, F. Pan, Z. Jiang, P. Zhang, X. Z. Cao, B. Wang, *J. Mater. Chem. A* **2015**, *3*, 19980-19988.

[20] J. H. Cavka, S. Jakobsen, U. Olsbye, N. Guillou, C. Lamberti, S. Bordiga, K. P. Lillerud, *J. Am. Chem. Soc.* **2008**, *130*, 13850-13851.

[21] Z. Wenjuan, H. Hongliang, Z. Chongli, L. Dahuan, *Phys.l Chem. Chem. Phys.* **2012**, *14*, 2317-2325.

[22] M. Golpour, M. Pakizeh, *Chem. Eng. J.* **2018**, *345*, 221-232.

[23] a) B. Ghalei, K. Sakurai, Y. Kinoshita, K. Wakimoto, Ali P. Isfahani, Q. Song, K. Doitomi, S. Furukawa, H. Hirao, H. Kusuda, S. Kitagawa, E. Sivaniah, *Nat. Energy* **2017**, *2*, 17086; b) S. R. Venna, M. Lartey, T. Li, A. Spore, S. Kumar, H. B. Nulwala, D. R. Luebke, N. L. Rosi, E. Albenze, *J. Mater. Chem. A* **2015**, *3*, 5014-5022; c) Z. Wang, H. Ren, S. Zhang, F. Zhang, J. Jin, *J. Mater. Chem. A* **2017**, *5*, 10968-10977.

[24] Q. Chen, Q. He, M. Lv, Y. Xu, H. Yang, X. Liu, F. Wei, *Appl. Surf. Sci.* **2015**, *327*, 77-85.

[25] H. C. Yang, R. Z. Waldman, M. B. Wu, J. Hou, L. Chen, S. B. Darling, Z. K. Xu, *Adv. Funct. Mater.* **2018**, *28*.

[26] E. M. Rundquist, C. J. Pink, A. G. Livingston, *Green Chem.* **2012**, *14*, 2197-2205.

[27] I. B. Valtcheva, S. C. Kumbharkar, J. F. Kim, Y. Bhole, A. G. Livingston, *J. Membr. Sci.* **2014**, *457*, 62-72.

[28] M. F. J. Solomon, Y. Bhole, A. G. Livingston, *J. Membr. Sci.* **2013**, *434*, 193-203.

[29] I. Soroko, A. Livingston, *J. Membr. Sci.* **2009**, *343*, 189-198.

[30] S. Kandambeth, B. P. Biswal, H. D. Chaudhari, K. C. Rout, S. Kunjattu H., S. Mitra, S. Karak, A. Das, R. Mukherjee, U. K. Kharul, *Adv.Mater.* **2017**, *29*.

[31] M. F. Jimenez-Solomon, Q. Song, K. E. Jelfs, M. Munoz-Ibanez, A. G. Livingston, *Nat. Mater.* **2016**, *15*, 760-767.

[32] X. Wang, L. Zhai, Y. Wang, R. Li, X. Gu, Y. D. Yuan, Y. Qian, Z. Hu, D. Zhao, *ACS Appl. Mater. Interfaces* **2017**, *9*.

[33] a) J. M. Hutchinson, *Prog. Polym. Sci.* **1995**, *20*, 703-760; b) I. Rose, C. G. Bezzu, M. Carta, B. Comesañagándara, E. Lasseuguette, M. C. Ferrari, P. Bernardo, G. Clarizia, A. Fuoco, J. C. Jansen, *Nat. Mater.* **2017**, *16*, 932.

[34] J. Kurchan, *Nature* **2005**, *433*, 222.

[35] S. L. Phua, L. Yang, C. L. Toh, D. Guoqiang, S. K. Lau, A. Dasari, X. Lu, *Acs Appl Mater Interfaces* **2013**, *5*, 1302-1309.

[36] L. Yu, J. F. Yang, B. Y. Guan, Y. Lu, X. W. Lou, *Angew. Chem. Int. Ed.* **2018**, *57*, 1-1.

[37] T. Wang, H. Qiblawey, E. Sivaniah, A. Mohammadian, *J. Membr. Sci.* **2016**, *511*, 65-75.

[38] a) G. Bargeman, J. B. Westerink, O. Guerra Miguez, M. Wessling, *Sep. Purif. Technol.* **2014**, *134*, 46-57; b) X. Liu, N. K. Demir, Z. Wu, K. Li, *J. Am. Chem. Soc.* **2015**, *137*, 6999-7002; c) Z. Tan, S. Chen, X. Peng, L. Zhang, C. Gao, *Science* **2018**, *360*, 518-521; d) J. Zhu, L. Qin, A. Uliana, J. Hou, J. Wang, Y. Zhang, X. Li, S. Yuan, J. Li, M. Tian, J. Lin, B. Van der Bruggen, *ACS Appl. Mater. Interfaces* **2017**, *9*, 1975-1986; e) H. Yi, X. Zhen, G. Chao, *Adv. Funct. Mater.* **2013**, *23*, 3693-3700; f) Z. Yuzhang, X. Wei, G. Shoujian, Z. Feng, Z. Wenbin, L. Zhaoyang, J. Jian, *Small* **2016**, *12*, 5034-5041; g) Y.J. Tang, Z.L. Xu, S.M. Xue, Y.M. Wei, H. Yang, *J. Membr. Sci.* **2016**, *498*, 374-384.

[39] a) A. K. Shukla, J. Alam, M. Alhoshan, L. A. Dass, M. R. Muthumareeswaran, *Sc. Rep.* **2017**, *7*, 41976; b) R,N. Zhang, M.R. He, D.H. Gao, Y.N. Liu, M.Y. Wu, Z.W. Jiao, Y.L. Su, Z.Y. Jiang, J. Membr. Sci, 2018,566 258–267.c

[40] H. Sun, X. Yang, Y. Zhang, X. Cheng, Y. Xu, Y. Bai, S. Lu, *J. Membr. Sci.* **2018**, *563*, 22-30.

[41] aS. Z. Pei, N. Widjojo, T. S. Chung, M. Weber, C. Maletzko, *J. Membr. Sci.* **2012**, *417-418*, 52-60; bQ. C. Xi, Z. Cong, X. W. Zhen, S. Lu, *J. Membr. Sci.* **2016**, *499*, 326-334.

[42] C. X. Yan, Q. C. Xi, J. Long, S. Lu, *J. Membr. Sci.* **2016**, *497*, 77-89.

Entry for the Table of Contents (Please choose one layout)

Layout 1:

RESEARCH ARTICLE

A facile technique to combine natural compounds and metal organic frameworks (MOFs) that produces a well-structured membrane with unparalleled separation performances in both nanofiltration modes was fabricated. Our designed membrane enables ultra-fast, low-pressure, precise separations for both solvent purification *via* organic solvent nanofiltration and desalination – key membrane-

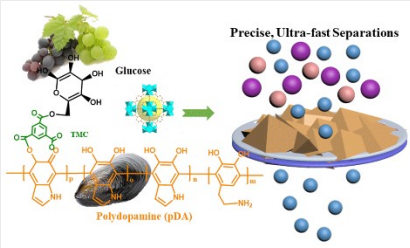

Yanqiu Zhang[a], Xiquan Cheng[b], Xu Jiang[a], Jeffrey J Urban[d], Cher Hon Lau[c], Lu Shao*[a,d]*

Page No. – Page No.

Ultrafast Dual-mode Precise Separation Membranes via Natural-driven Interfacial-confined Reaction

Layout 2:

RESEARCH ARTICLE

((Insert TOC Graphic here))

*Author(s), Corresponding Author(s)**

Page No. – Page No.

Title

Text for Table of Contents